Journal of Zhejiang University-SCIENCE A (Applied Physics & Engineering)
ISSN 1673-565X (Print); ISSN 1862-1775 (Online)
www.zju.edu.cn/jzus; www.springerlink.com
E-mail: jzus@zju.edu.cn

Numerical simulation of gas-liquid flow through a 90° duct bend with a gradual contraction pipe*

Dong-fang HU[1], Zheng-liang HUANG[†‡1], Jing-yuan SUN[1], Jing-dai WANG[1], Zu-wei LIAO[1], Bin-bo JIANG[1], Jian YANG[2], Yong-rong YANG[1,2]

([1]*State Key Laboratory of Chemical Engineering, College of Chemical and Biochemical Engineering, Zhejiang University, Hangzhou 310027, China*)

([2]*Shanghai Key Laboratory of Catalysis Technology for Polyolefins, Shanghai 200062, China*)

[†]E-mail: huangzhengl@zju.edu.cn

Received Jan. 13, 2016; Revision accepted July 28, 2016; Crosschecked Feb. 7, 2017

Abstract: The effect of a gradual contraction pipe (GCP) on gas-liquid flow in a circular-sectioned horizontal to vertical 90° duct bend was investigated by computational fluid dynamics (CFD) simulation. The hydrodynamics of gas-liquid flow in 90° duct bends with and without a GCP in the vertical section were compared using a 3D steady Eulerian-Eulerian approach. The predicted static pressure in the vertical section of the pipes and the pressure drop in the whole pipe were consistent with experimental data. Results of simulations showed that liquid could distribute more uniformly at the exit of the pipe with a GCP. The increased uniformity was accompanied by an increase in pressure drop by a factor of less than 10% compared to the pipe without a GCP. The position of minimum pressure in the bend was changed by the GCP. A GCP can alter the trajectories of the fluid and secondary flow. As a result, the fluid can quickly reach a steady state downstream from the bend.

Key words: 90° duct bend; Contraction; Computational fluid dynamics (CFD); Uniform distribution; Hydrodynamics
http://dx.doi.org/10.1631/jzus.A1600016 **CLC number:** O359.1

1 Introduction

In many industrial processes, pipelines are used to convey supplies. A comprehensive understanding of fluid dynamics in pipes is essential for good pipe design and pipeline arrangements. Due to limitations of installation space, bends are frequently used to change the direction of a pipe. In this way, the fluid can be transported to the desired delivery position. However, the centrifugal effect arising from a bend leads to separation of a multiphase fluid (Akilli *et al*., 2001). Therefore, a long straight pipe is required to stabilize the separated fluid downstream of the bend (Weske, 1948). However, the length of the straight pipe is limited in some processes. For example, during the olefin polymerization in a fluidized bed reactor in condensed mode operation, the vertical pipe connected to the inlet of the reactor is not long enough to stabilize the separated gas-liquid after flowing through the bend. This may cause maldistribution of liquid in the reactor. Heat generated by the reaction cannot then be taken away, which leads to hotspots in polymer agglomeration. Also, the inner wall of the reactor may be eroded in the areas of high liquid content areas. Consequently, it is important to study

‡ Corresponding author

* Project supported by the National Natural Science Foundation of China (No. 91434205), the National Science Fund for Distinguished Young Scholars (No. 21525627), the Zhejiang Provincial Natural Science Foundation of China (No. LR14B060001), and the Specialized Research Fund for the Doctoral Program of Higher Education of China (No. 20130101110063)

ORCID: Zheng-liang HUANG, http://orcid.org/0000-0002-8457-6394

the fluid dynamics in a duct bend and propose a valid way to make liquid distribute uniformly in the reactor, thereby avoiding agglomeration and extending the service life of the reactor.

Previous studies of multiphase flow in curved pipes can be separated into those focusing on gas-solid or gas-liquid systems in circular or non-circular pipes. Most researchers have focused on gas-solid flow in a 90° duct bend. They have observed the phenomenon of particle rope and have estimated the pressure drop due to the bend, the fluid velocity distribution in the pipe, and the fluctuation force imposed on the pipe by the fluid (Akilli *et al*., 2001; Spedding *et al*., 2006; Kuan *et al*., 2007; Njobuenwu *et al*., 2012; Vashisth and Grace, 2012; Zhang *et al*., 2012). The phenomenon of gas-liquid flowing through a 90° duct bend is similar to that of gas-solid. A variety of studies has focused on the effect of a bend on the hydrodynamics of gas-liquid flow in a pipe. Sroka and Forney (1989) conducted an experiment to investigate the gas-liquid hydrodynamics downstream from a 90° bend, and discovered that the fluid fluctuation was more intense than that in a straight pipeline. This was attributed to the bend. Some researchers have discussed the pressure drop caused by a bend based on the experimental or simulation results (Spedding and Benard, 2007; Alizadehdakhel *et al*., 2009; Crawford *et al*., 2009; Kim *et al*., 2010). They constructed some models to predict the pressure drop for engineering design. Wang *et al.* (2003; 2004) proposed new flow patterns to describe the effect of a return bend on the transition of a two-phase flow pattern via visual observation. They found that the flow pattern was related to the curvature of the bend. Liu *et al.* (2012) conducted an experiment to study the fluctuation in a two-phase flow by a 90° bend. The fundamental mechanisms and characteristics of the excitation force caused by two-phase flows were obtained by eliminating the influence of the vibration of the bend. Kim *et al.* (2007) investigated the geometric effects of a 90° bend on the distribution of local two-phase flow parameters and its transport characteristics in a horizontal bubbly flow. The bend induced significant oscillations in the flow in both the vertical and horizontal directions of the tube cross-section. The transport of the 1D interfacial area concentration and the void fraction along the flow were also affected by the bend.

Although the results obtained by the above studies give valuable insights into the effects of a pipe with a bend, few studies have focused on a method to solve the phase separation caused by a bend. Bilirgen and Levy (2011) assessed techniques for dispersing the severe particle stratification caused by flow through a 90° duct bend. According to their results, each type of flow mixer has its own shortcomings. Fan *et al.* (2002) carried out a theoretical study of a ribbed bend to protect duct bends against erosion in gas-solid flows. The results of these two studies showed that a proper internal can help redistribute the solid downstream of the bend. However, as some of the internals are installed in on the inside wall of the pipe, it is hard to check the condition of the internals when the pipe is working. The variation in the flow dynamics caused by the internals had been less well studied.

In this study, we propose mounting a gradual contraction pipe (GCP) in the straight pipe downstream of a bend to redistribute the fluid. A GCP is widely used in cryocoolers to enhance the heat transfer owing to the oscillatory flow in a GCP (Shiraishi *et al*., 2002; Holley and Faghri, 2005; He *et al*., 2007; Yang, 2009). This can strengthen the turbulence intensity in a pipe. Ahmadpour *et al*. (2016) presented a detailed numerical simulation of two-phase air and water flow through gradual expansions/contractions. They found that the gradual expansions/contractions could clearly change the pressure and velocity of the two phases. So a GCP could be an effective device to adjust the flow of fluid downstream of a bend. To verify our idea, a 3D steady Eulerian-Eulerian approach was adopted to simulate fluid flow in a 90° duct bend with a GCP. The simulation method was validated by the static pressure obtained by experiment. We discuss in detail the effect of the GCP on the hydrodynamics of gas-liquid two-phase flow in a 90° duct bend. This study provides some valuable insights for pipeline design in industrial applications.

2 Experiment apparatus and materials

The experimental facilities are shown schematically in Fig. 1 together with the adopted coordinate system whose origin is located at the center of the outlet plane of the bend. Air and water was used as the

test fluid in all the experiments. Air was injected into the apparatus by an air compressor. Water was pumped into the pipeline through a nozzle so as to ensure it was distributed uniformly at the pipe inlet.

Two circular horizontal to vertical 90° duct bends were used in the experiments, one with a GCP in the vertical segment (the C pipe) and the other without (the NOC pipe). The internal diameters of the pipes were D=140 mm. They comprised a 90° bend of curvature radius R_c=75 mm (R_c/D=0.54), and horizontal and vertical tangents of 12D and 3.78D. The detailed dimensions of the C pipe are shown in Fig. 1. Its diameter was reduced to D'=0.85D downstream of the GCP.

Since the aim of this work was to offer some suggested improvements for the industry, it was necessary to ensure that the flow pattern in the experiments was the same as that in industrial apparatus. In experiments, the gas velocity v_g and liquid mole fraction x_l were set in the range of 9.93 to 14.40 m/s and 0 to 15.53%, respectively. So the flow pattern in the experiment was mist flow according to the flow pattern map of Baker (1954). The static pressure near the vertical section wall of the pipe was measured by a U tube to validate computational fluid dynamics (CFD) simulation. The pressure taps were located 1 mm from the inner and outer side walls with elevations y/D=0.2, 0.5, 0.85, 1.2, 1.7, 2.0, 2.4, 2.6, 3.0, and 3.8.

3 Mathematical models

3.1 Governing equations

The Eulerian-Eulerian two fluid model has been reported to be an appropriate way to simulate a dispersed liquid spray, and the solutions obtained by this method are similar to those obtained by the Eulerian-Lagrangian approach (Burger *et al*., 2002; Moukalled and Darwish, 2008; Li *et al*., 2010; Zhang *et al*., 2013). The main shortcomings of the Eulerian-Lagrangian method are large memory and central processing unit (CPU) requirements. So the 3D Eulerian-Eulerian method was used in this study. The governing equations shown below were calculated by a commercial CFD software Fluent 6.3.13.

Continuity equation is

$$\frac{\partial}{\partial t}(\rho_i\alpha_i)+\nabla\cdot(\rho_i\alpha_i\boldsymbol{v}_i)=0, \tag{1}$$

where i represents g or l, ρ_i is the density of phase i, α_i is the volume fraction of phase i, and $\boldsymbol{v}_i$ is the velocity of phase i.

Momentum equation is

$$\frac{\partial}{\partial t}(\rho_i\alpha_i\boldsymbol{v}_i)+\nabla\cdot(\rho_i\alpha_i\boldsymbol{v}_i\boldsymbol{v}_i) = -\alpha_i\nabla p+\nabla\cdot\boldsymbol{\tau}_i+\rho_i\alpha_i g+M_i, \tag{2}$$

where $\boldsymbol{\tau}_i$ is the stress tensor, and M_i is the force between the gas and liquid, including the drag force, buoyancy, virtual gravity, turbulent dispersion, and wall force. The magnitude of the drag force is higher than that of other kinds of force because of the mist flow in the pipe. So only the drag force was considered in this study. The Schiller-Naumann (Schiller and Naumann, 1935) method was used as model for drag between the gas and liquid.

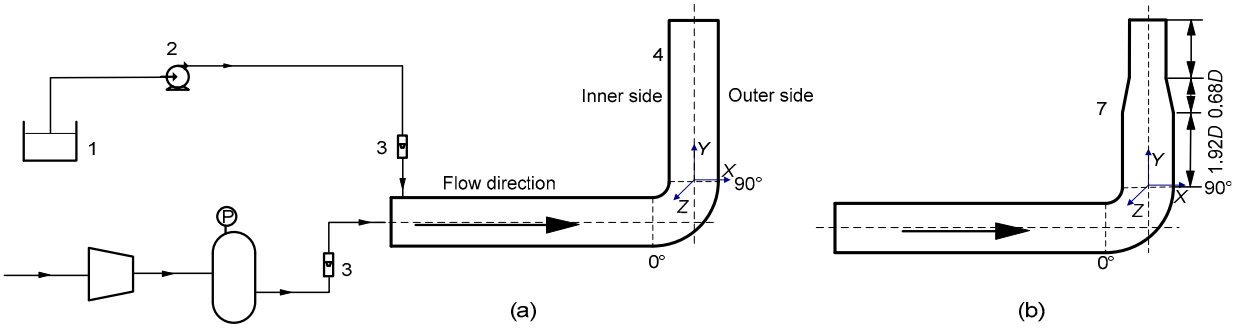

Fig. 1 Schematic diagram of the experimental facility
1: Buffer tank; 2: Pump; 3: Flow meter; 4: NOC pipe; 5: Air compressor; 6: Tank; 7: C pipe

$$K_{\mathrm{gl}}=\frac{\alpha_{\mathrm{g}}\alpha_{\mathrm{l}}\rho_{\mathrm{l}}f}{\tau_{\mathrm{l}}}, \tag{3}$$

where K_{gl} is the drag force between the gas and liquid.

$$\tau_{\mathrm{l}}=\frac{\rho_{\mathrm{l}}d_{\mathrm{l}}^2}{18\mu_{\mathrm{l}}}, \tag{4}$$

$$f=\frac{C_{\mathrm{D}}Re}{24}, \tag{5}$$

where d_{l} is the diameter of the droplet, Re is the Reynolds number, and μ_{l} is the liquid viscosity. The drag coefficient C_{D} is given by

$$C_{\mathrm{D}}=\begin{cases}24(1+0.15Re^{0.687})/Re, & Re<1000,\\ 0.44, & Re\geq 1000.\end{cases} \tag{6}$$

The k-ε model (Launder and Spalding, 1972) is used to estimate the turbulence of the gas phase by taking into account the effect of the liquid phase. The transport equations for k and ε were

$$\frac{\partial}{\partial t}(\alpha_{\mathrm{g}}\rho_{\mathrm{g}}k)+\nabla\cdot(\alpha_{\mathrm{g}}\rho_{\mathrm{g}}\boldsymbol{v}_{\mathrm{g}}k)=\nabla\left(\alpha_{\mathrm{g}}\frac{\mu_{\mathrm{g},t}}{\sigma_k}\nabla k\right)+\alpha_{\mathrm{g}}G-\alpha_{\mathrm{g}}\rho_{\mathrm{g}}\varepsilon+\Pi_{\mathrm{l},k}, \tag{7}$$

$$\frac{\partial}{\partial t}(\alpha_{\mathrm{g}}\rho_{\mathrm{g}}\varepsilon)+\nabla\cdot(\alpha_{\mathrm{g}}\rho_{\mathrm{g}}\boldsymbol{v}_{\mathrm{g}}\varepsilon)=\nabla\left(\alpha_{\mathrm{g}}\frac{\mu_{\mathrm{g},t}}{\sigma_k}\nabla\varepsilon\right)+\alpha_{\mathrm{g}}\frac{\varepsilon}{k}(C_1G-C_2\rho_{\mathrm{g}}\varepsilon)+\Pi_{\mathrm{l},\varepsilon}, \tag{8}$$

where k is the turbulent kinetic energy, ε is the dissipation rate of turbulent kinetic energy, and Π is the additional term.

3.2 Initial and boundary conditions for simulation

The computed flow domain was constructed using hexahedral cells with the grid sensitivity study shown in Fig. 2. A finer mesh for the boundary layer of the pipe was constructed to improve the accuracy of the flow simulation in the wall-adjacent region. The selected cell number was 375 464 for considering both the accuracy and time used for calculation. In this study, the droplet diameter was simplified to a constant value at the inlet, which is closely related to the *We* number (Kolmogorov, 1949):

$$We=\frac{2\rho_{\mathrm{g}}}{\sigma_{\mathrm{l}}}E^{2/3}d_{\max}^{5/3}, \tag{9}$$

where E is the turbulent kinetic energy, and σ_{l} is the surface tension of the liquid. The maximal stable droplet diameter $d_{\max}$ is

$$d_{\max}=0.725\left(\frac{\sigma_{\mathrm{l}}}{\rho_{\mathrm{g}}}\right)^{3/5}E^{-2/5}. \tag{10}$$

The initial and boundary conditions for simulation are shown in Table 1.

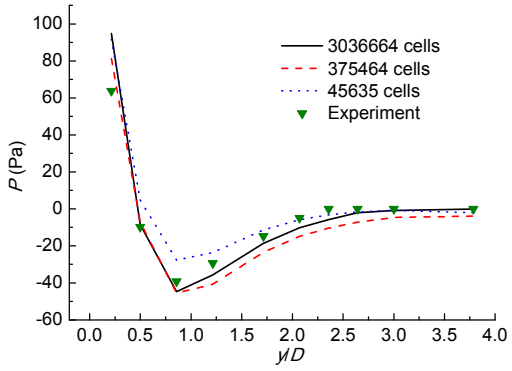

Fig. 2 Effect of cell number on static pressure, P (v_{g}= 14.4 m/s, x_{l}=0)

Table 1 Initial and boundary conditions for simulation

Parameter	Value/Comment
Inlet boundary condition	
Range of gas velocity (m/s)	9.93–14.40
Range of liquid mole fraction (%)	0–15.53
Outlet boundary condition	Outflow
Wall boundary condition	
Gas phase	No slip
Liquid phase	No slip

3.3 Numerical procedure for simulation

A steady-state simulation was performed using the commercial CFD software, Fluent 6.3.13, in double precision mode. A pressure based segregated

method was used, with a semi-implicit method for pressure-linked equations (SIMPLE) scheme for pressure-velocity coupling. Based on the preliminary work, the standard k-ε turbulence model with fast computation speed and ease of convergence was selected to solve the transport equations of k and ε. The flow in the near-wall region is solved by the standard wall function to achieve high accuracy of numerical solutions in the entire domain. The first order upwind scheme was used for the spatial discretization of all variables. The residual convergence criterion was set to 10^{-4} for all equations.

4 Results and discussion

4.1 Model validation

To validate the simulation model, the predicted static pressure in the vertical sections of the pipes was compared with the experimental results. Some typical simulation results are presented in Fig. 3 with corresponding experimental results from the NOC pipe for comparison. The simulation results agree reasonably well with the experimental data, except at the lower y/D of the inner side. The pressure tap must be parallel to the flow direction of the fluid when measuring the static pressure of the fluid. However, the backflow region at the lower y/D of the inner side causes complexity in the fluid flow direction. It is hard to keep the pressure taps parallel to the flow direction of the fluid, so the measured static pressure is lower than the simulation results for the inner side. In contrast, the fluid flow direction is approximately parallel to the pipe wall of the outer side. Therefore, the experimental and simulation results matched well on the outer side.

Large numbers of empirical correlations have been obtained to predict the pressure drop of turbulent gas liquid flow in 90° bends. Azzi *et al*. (1999) gave a detailed review of empirical correlations of pressure drop. The empirical model of Paliwoda (Paliwoda, 1992) was selected from among those correlations to validate the numerical results of the pressure drop ΔP between the entrance and the exit of the bend. The correlation was given as

$$\frac{\Delta P}{\Delta P_g}=\left[\varphi+2.7(1-\varphi)x^*\right](1-x^*)^{0.333}+x^{*2.276},$$

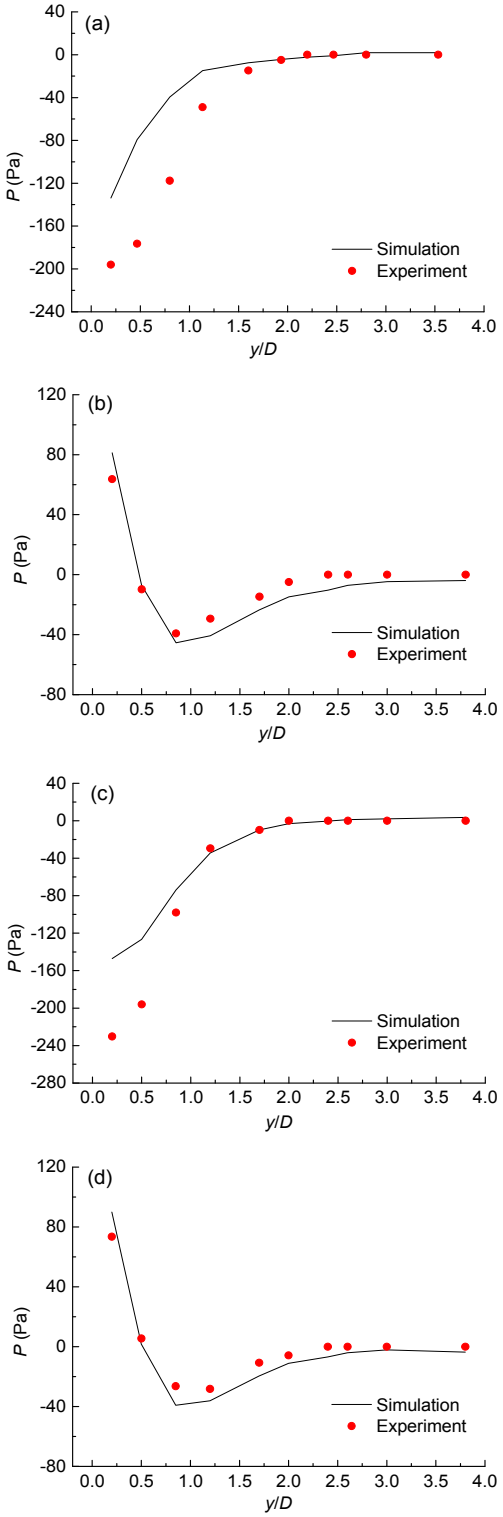

Fig. 3 Comparison of predicted and experimental static pressure in the vertical section

(a) Inner side of the NOC pipe, v_g=14.4 m/s, x_l=0; (b) Outer side of the NOC pipe, v_g=14.4 m/s, x_l=0; (c) Inner side of the NOC pipe, v_g=14.4 m/s, x_l=7.71%; (d) Outer side of the NOC pipe, v_g=14.4 m/s, x_l=7.71%

$$\varphi=\frac{\rho_g}{\rho_l}\left(\frac{\mu_l}{\mu_g}\right)^{0.25}, \quad (11)$$

where x^* is the mass fraction of gas. The single-phase air flow pressure drop ΔP_g is obtained from

$$M=\Delta P_g/(\rho v_g^2), \quad R_c/D=0.54, M=0.286. \quad (12)$$

From Fig. 4 we can see that the numerical results showed good agreement with Paliwoda's empirical correlation.

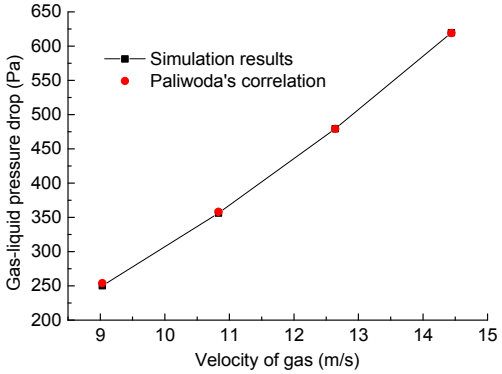

Fig. 4 Comparison between the numerical results and Paliwoda's empirical correlation

4.2 Effect of the GCP on fluid distribution

In this section, to check the effect of the GCP on the uniformity of liquid at the exit of the pipe, the results of the C pipe are compared with those of the NOC pipe and in scenarios with vertical segments of different lengths.

4.2.1 Distribution of liquid

Fig. 5 presents the normalized liquid volume fraction along the radial direction on the cross-section at different elevations. The normalized liquid volume fraction is expressed as

$$\phi_{nl}=\frac{\phi_l}{\phi_0}, \quad (13)$$

where ϕ_0 is the liquid volume fraction at the inlet.

The x/r=0, x/r=1, and x/r=−1 in Fig. 5 represent the center, inner side, and outer side of the cross-section, respectively, where r is the radius of the pipe and x is the X coordinate. The flow pattern of the fluid is greatly altered by the centrifugal force when it flows through the bend. Most of the liquid would be thrown to the outer side wall of the bend, so the liquid volume fraction is higher near x/r=1 than near x/r=−1 (Fig. 5). Besides, it's even higher near x/r=1 in the GCP. Fig. 5a shows that the liquid volume fraction increases with increasing of elevation when $-1<x/r<-0.2$, and slightly decreases when $0.8<x/r<1$, indicating that liquid flows from the outer side to the inner side in the vertical section. Fig. 5b shows the same profile as Fig. 5a. However, the liquid volume fraction along the radial direction is more uniform in the exit plane of the C pipe.

In the simulation, 16 equally distributed points shown in Fig. 6 were selected to investigate the distribution of liquid near the wall of the vertical section. Among these points, point 1 was on the outer side and point 9 was on the inner side of the pipe. Fig. 7 shows the normalized liquid distribution near the wall of the

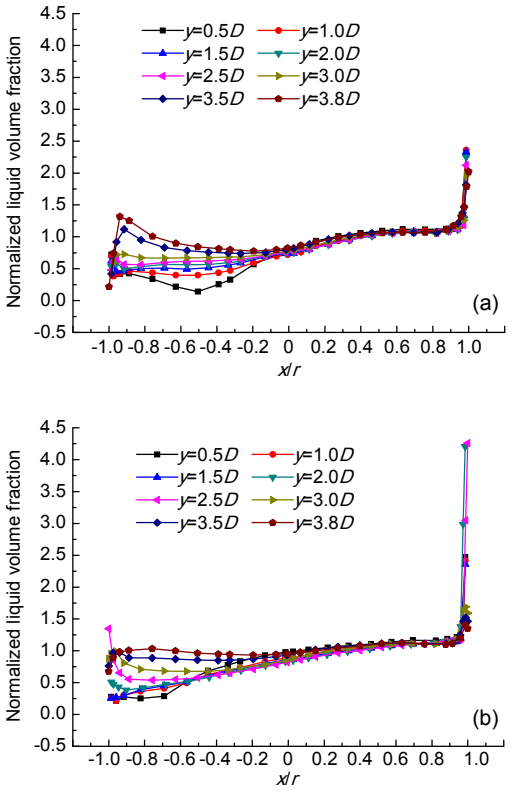

Fig. 5 Liquid volume fraction along the radial direction of the cross-section at different elevations (v_g=14.4 m/s, x_l=7.71%): (a) NOC pipe; (b) C pipe

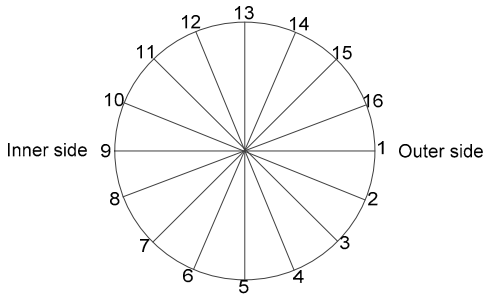

Fig. 6 Schematic diagram of sampling points distributed near the wall of the circular section

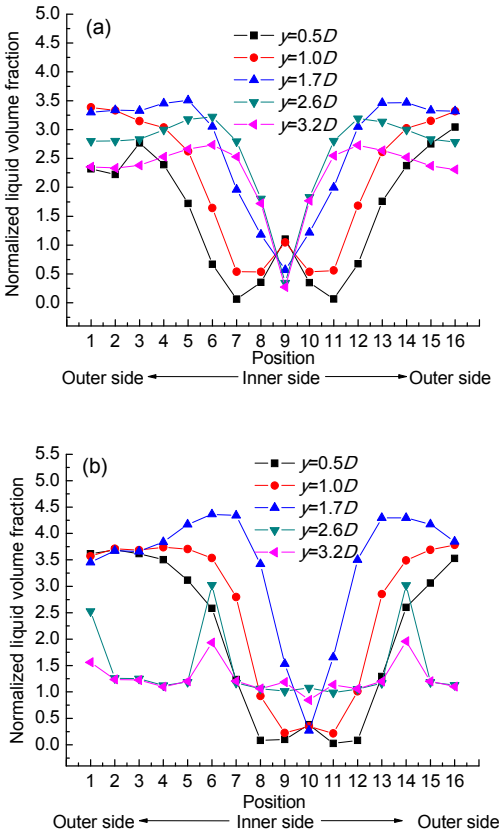

Fig. 7 Liquid distribution near the wall of the vertical section on the circular section at different elevations (v_g=14.4 m/s, x_l=7.71%): (a) NOC pipe; (b) C pipe

circular section at different elevations. The liquid becomes more and more uniformly distributed on the circular section with increasing of elevation. Also, the liquid distribution is more uniform on the exit plane of the C pipe. Fig. 7 further reveals that the liquid volume fraction of point 9 is higher than those of the points beside it on the y=0.5D and y=1.0D planes, and is responsible for the backflow of liquid there. The gradient between point 9 and the points beside it is small in the C pipe owing to the small amount of liquid backflow. The liquid volume fractions of points 6 and 14 are higher than those of the points beside them on the y=2.6D and y=3.2D planes (Fig. 7b). This is because points 6 and 14 are the stagnation points of the liquid, since a lot of liquid moves from the outer to the inner side.

The variation coefficients of the liquid volume fraction at exits of the two pipes for different experimental conditions are compared in Fig. 8. The definition of the variation coefficient V is

$$V=\frac{\sigma_s}{\overline{S}}, \tag{14}$$

where σ_s is the standard deviation, and $\overline{S}$ is the average value of a set of data. V estimates the uniformity of a set of data.

Fig. 8 shows that the variation coefficient of the C pipe is lower than that of the NOC pipe within the range of the experimental conditions applied in this study, indicating that liquid is more uniform at the exit of the C pipe. The variation coefficients of the two pipes remain almost constant with increasing of liquid volume fractions (Fig. 8a). However, the separation phenomenon becomes more and more severe with increasing of gas velocity in the vertical section. The variation coefficient of the NOC pipe increases more rapidly than that of the C pipe (Fig. 8b). This shows that the variation coefficient is more sensitive to gas velocity than the liquid volume fraction in the NOC pipe.

To sum up, all the results of the experiments and simulations show that the liquid is more uniform at the exit of the C pipe owing to the GCP.

4.2.2 Effect of increasing the length of the vertical section

According to the theory of gas-liquid two-phase fluid mechanics, a straight pipe with length of about 10D is required for fully developed flow (Weske, 1948). However, this requirement cannot be met in some industry processes due to space limitations, as in the case of a pipeline connecting the inlet of a polyolefin fluidized bed reactor. In this section, the results from four scenarios with increasing length of the vertical section of the NOC pipe are compared

with the results from the C pipe. The variation coefficients of the liquid volume fraction at exits of the pipes are compared in Table 2 for all scenarios. The variation coefficient of the NOC pipe decreases with increasing length of the vertical section. However, the value of the C pipe is still lower even when a 4*D* straight pipe is added, indicating that the GCP can help redistribute liquid and decrease the length of vertical section required for uniform liquid distribution. In this way, the cost of space and material could be saved in industrial applications.

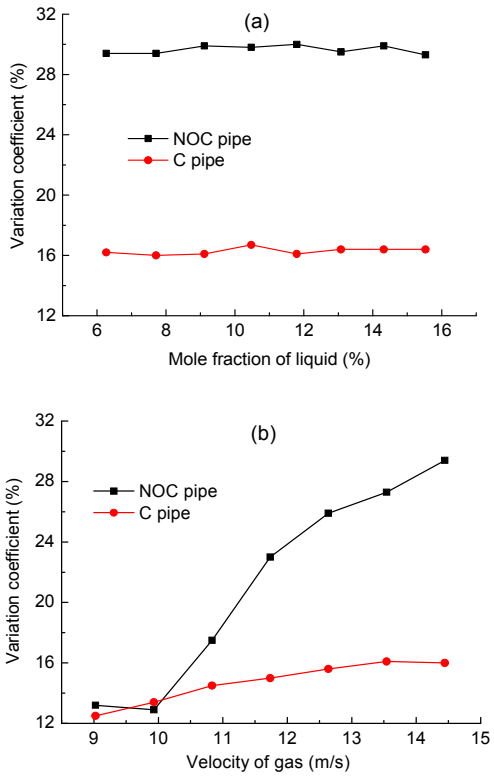

Fig. 8 Variation coefficient of liquid volume fraction at the exits of the two pipes: (a) v_g=14.4 m/s; (b) x_l=7.71%

Table 2 Comparison of variation coefficients in scenarios involving different lengths of the vertical section (v_g= 14.4 m/s, x_l=7.71%)

Scenario	*V*
NOC pipe	29.4
NOC pipe (*D* added)	46.2
NOC pipe (2*D* added)	31.1
NOC pipe (3*D* added)	26.6
NOC pipe (4*D* added)	20.0
C pipe	16.0

4.3 Effect of the GCP on fluid hydrodynamics

To find the mechanism by which the GCP redistributes the fluid, the hydrodynamics of the two pipes were investigated.

4.3.1 Pressure

Pressure is the most important hydrodynamic parameter for fluid flow in the pipe. The simulated static pressure near the inner and outer side walls of the entire pipe is shown in Fig. 9, where θ is the polar angle of the bend. Figs. 9a and 9b show the same trend with a large pressure gradient in the bend. The centrifugal force caused by the bend results in a decrease in horizontal velocity and an increase in static pressure in the first half of the bend. The static pressure decreases after the maximum value is reached, indicating that the fluid flow direction gradually adjusts to the shape of the outer side wall of the bend. The static pressure decreases in the first half of the inner side of the bend. This is because the fluid is not blocked by the wall there. Although the inner side wall of the bend curves upwards, the static pressure increases as the fluid still flows towards the horizontal. Similar results have been noted by Rutten *et al*. (2001) and Njobuenwu *et al*. (2012).

Fig. 9 also reveals that the pressure gradient between the inner and outer sides of the bend in the C pipe is greater than that in the NOC pipe. This is because the gas velocity on the inner side of the C pipe's bend is higher than that of the NOC pipe. The minimum static pressure in the NOC pipe is located at 45° of the bend, while in the C pipe this shifts to 60°, because the flow direction of the fluid changes towards the vertical section early on the inner side of the bend of the C pipe. Moreover, the GCP changes the pressure not only in the bend, but also in the straight segments of the pipe.

4.3.2 Secondary flow

A secondary flow forms downstream of a bend when a fluid flows through the bend (Yao and Berger, 1975; Chen *et al*., 2003). A secondary flow is a relatively minor flow superimposed on the primary flow and contributes to the distribution of fluid in the pipe. Vashisth and Grace (2012) found that a secondary flow can help disperse the particle rope. Table 3 shows the secondary flow on the cross section at different elevations of the two pipes in this study. The

arrows in the figures stand for the radial gas velocity vectors. There were only two little vortexes near the wall of the inlet plane (Table 3). On the 2*D* plane, just under the GCP in the C pipe, the secondary flow appears to be double symmetric vortexes, the centers of which are close to the outer side wall of the two pipes. The centers are closer to the outer side wall of the C pipe. Then they move to the center of the cross section on the outlet plane. The figures show that there is a strong secondary motion driven along a thin region adjacent to the pipe wall due to the excess of the radial pressure gradient over that required for circular motion (Iacovides *et al*., 1990). Also, there is a stagnation point near the inner side of the 2*D* and outlet planes at which the fluid starts to eject towards the center of the cross section. Table 3 shows that the maximum velocity of secondary flow in the C pipe is higher than that in the NOC pipe owing to the decrease in the flow area, indicating that the radial movement of the fluid is enhanced by the GCP.

4.3.3 Liquid velocity

In this section, we discuss the liquid velocity in the vertical section to illustrate the effect of the GCP

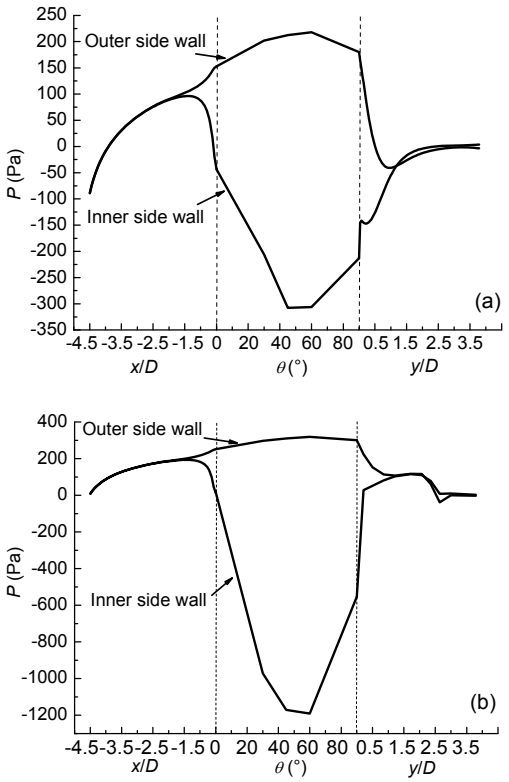

Fig. 9 Static pressure distribution along the whole pipe (v_g=14.4 m/s, x_l=7.71%): (a) NOC pipe; (b) C pipe

Table 3 Secondary flow at different elevations: v_g=14.4 m/s, x_l=7.71% (velocity unit: m/s)

Elevation	Secondary flow (NOC pipe)	Secondary flow (C pipe)
y=0 mm	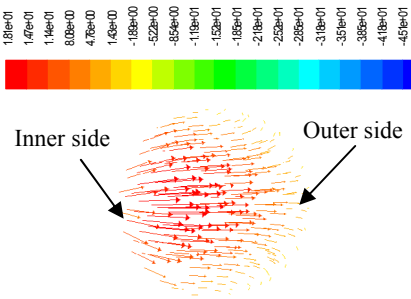	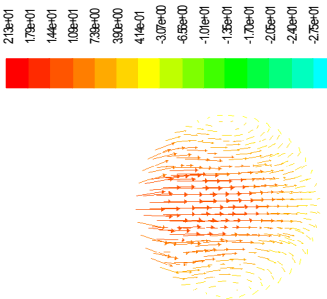
y=2*D*	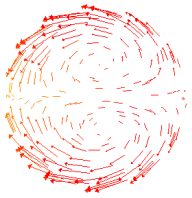	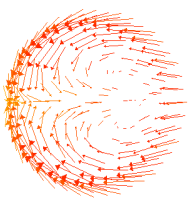
Outlet	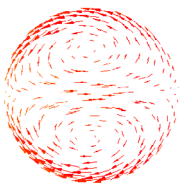	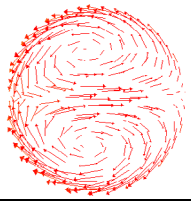

on the liquid flow pattern. The vertical liquid velocity contours of the C and NOC pipes are presented in Fig. 10, together with the amplified vector diagrams for the local region. There is a backflow zone near the bend exit of the two pipes owing to the secondary flow (Vashisth and Grace, 2012). The backflow velocity in the NOC pipe is higher than that in the C pipe. The reason for this is that more gas can flow upwards along the inner side of the vertical section after flowing through the bend of the C pipe. Fig. 10 also reveals that the liquid velocity in the horizontal section is affected by the GCP.

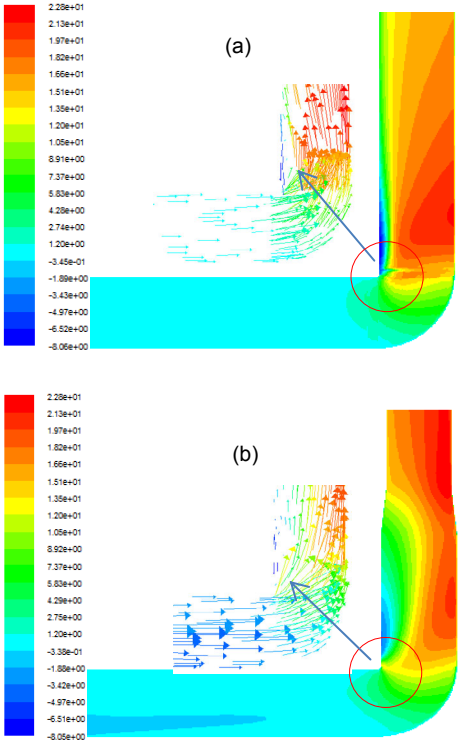

Fig. 10 Liquid velocity (m/s) in the vertical direction (v_g=14.4 m/s, x_l=7.71%): (a) NOC pipe; (b) C pipe

In Fig. 11, the liquid velocity on the inner and outer sides of the vertical section is plotted against the elevations. When liquid enters the bend of the NOC pipe, it is deflected from the horizontal and rushes to the outer side. This results in an initial increase in liquid velocity near the outer side of the vertical section. The liquid velocity then decreases as the liquid moves towards the inner side. As for the inner side of the vertical section, the velocity drops with the increase in static pressure in the backflow region. It begins to increase as the liquid flows from the outer side. It is clear that the liquid velocity profiles of the C pipe are the same as that of the NOC pipe below the GCP. However, the velocity increases in the GCP owing to the decrease in the flow area. The movement of liquid in the vertical section is swirl-shaped due to the secondary flow, which is similar to the results found by Weske (1948), Tunstall and Harvey (1968), and Kim *et al*. (2007). The velocity gradient between the inner and outer sides of the C pipe's exit plane is clearly smaller than that of the NOC pipe.

We conclude that the GCP can greatly change the flow pattern of liquid and that the distribution of liquid velocity is more uniform at the exit of the C pipe.

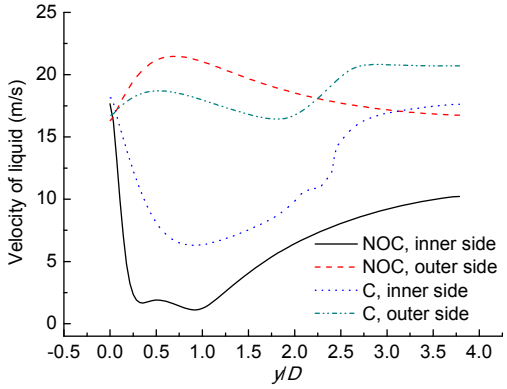

Fig. 11 Liquid velocity on the inner and outer sides of the vertical section (v_g=14.4 m/s, x_l=7.71%)

4.3.4 Turbulent kinetic energy

Turbulent kinetic energy (k) is the characterization of turbulence intensity of the fluid, and can indicate the distribution of the fluid and flow stability. It is defined as

$$k/m=\frac{1}{2}\left(\overline{u'^2}+\overline{v'^2}+\overline{w'^2}\right), \tag{15}$$

where m is the mass of the fluid, and u', v', and w' are the components of the fluctuating velocity.

Fig. 12 shows the distribution of k along the inner and outer sides of the vertical section. On the outer side, k increases at first and then decreases with increasing elevation. Because the gas velocity decreases with the increase in elevation in the backflow zone, k decreases at first on the inner side. It increases as the fluid moves from the outer to the inner side, and

then drops with the decrease in fluid velocity. Also, k rises slightly on both sides above $2D$, but the inner side lags behind the outer side. This is the result of the fluid flowing from the outer to the inner side. Fig. 12 shows that the profiles of k are similar for the two pipes. However, the gradient between the inner and outer sides of the C pipe is higher than that of the NOC pipe. We conclude that the flow pattern near the vertical pipe wall is greatly altered by the GCP.

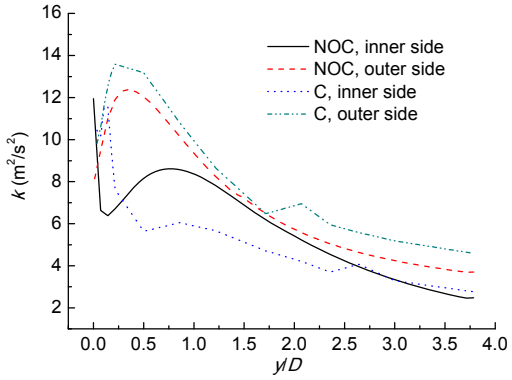

Fig. 12 Distribution of k along the inside and outside of the vertical section (v_g=14.4 m/s, x_l=7.71%)

Fig. 13 shows the distribution of k along the X axis on the cross section at different elevations. Fig. 13b resembles Fig. 13a in that k decreases with increasing elevation owing to the loss of energy. They both illustrate that an axially symmetric k profile is reestablished downstream of the bend. Fig. 13b shows the fluid reaches a steady state in the C pipe more quickly than that in the NOC pipe. Therefore, the results of this study suggest that the GCP can help stabilize the unsteady fluid within a short time.

5 Conclusions

We investigated the hydrodynamics of gas-liquid flow in two different kinds of circular horizontal to vertical 90° duct bends, one with a GCP in the vertical section and the other without. The applied numerical method was a 3D steady Eulerian-Eulerian approach with a standard k-ε turbulent model and a Schiller-Naumann gas-liquid drag model. The simulation results showed good agreement with the experimental data. Liquid was uniformly distributed at the exit of the C pipe. The pressure in the C pipe was greatly

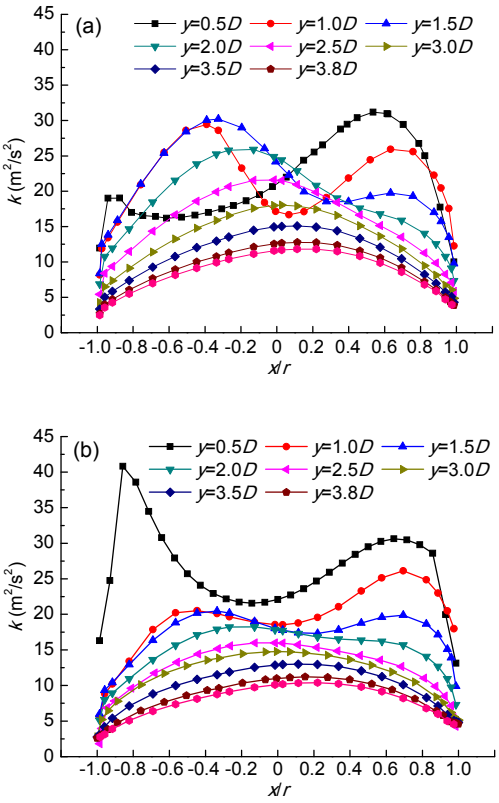

Fig. 13 Distribution of k along the X axis on the cross section at different elevations (v_g=14.4 m/s, x_l=7.71%): (a) NOC pipe; (b) C pipe

altered by the GCP as well as the trajectories of the fluid and secondary flow, so a lot of liquid could move from the outer to the inner side to reach a steady state quickly. Hence, with a GCP, a reactor downstream of the duct bend could operate safely. The GCP causes an increase in pressure drop by a factor of less than 10% in the C pipe compared to the pressure in the NOC pipe. To sum up, this study was a preliminary attempt to investigate the effect of a GCP on fluid redistribution downstream of a bend. Further work should be done to determine the relation between the structure of a GCP and its effectiveness, including the contraction ratio, length, and location of a GCP in the vertical segment.

References

Ahmadpour, A., Noori Rahim Abadi, S.M.A., Kouhikamali, R., 2016. Numerical simulation of two-phase gas–liquid flow through gradual expansions/contractions. *International Journal of Multiphase Flow*, **79**:31-49. http://dx.doi.org/10.1016/j.ijmultiphaseflow.2015.10.008

Akilli, H., Levy, E.K., Sahin, B., 2001. Gas-solid flow behavior in a horizontal pipe after a 90 degrees vertical-to-horizontal elbow. *Powder Technology*, **116**(1):43-52. http://dx.doi.org/10.1016/S0032-5910(00)00360-0

Alizadehdakhel, A., Rahimi, M., Sanjari, J., *et al*., 2009. CFD and artificial neural network modeling of two-phase flow pressure drop. *International Communications in Heat and Mass Transfer*, **36**(8):850-856. http://dx.doi.org/10.1016/j.icheatmasstransfer.2009.05.005

Azzi, A., Friedel, L., Belaadi, S., 1999. Two-phase gas/liquid flow pressure loss in bends. *Forschung im Ingenieurwesen*, **65**(7):309-318. http://dx.doi.org/10.1007/BF03035112

Baker, O., 1954. Simultaneous flow of oil and gas. *Oil Gas Journal*, **53**(1):85-95.

Bilirgen, H., Levy, E.K., 2011. Mixing and dispersion of particle ropes in lean phase pneumatic conveying. *Powder Technology*, **119**(2-3):134-152. http://dx.doi.org/10.1016/S0032-5910(00)00413-7

Burger, M., Klose, G., Rottenkolber, G., *et al.*, 2002. A combined Eulerian and Lagrangian method for prediction of evaporating sprays. *Journal of Engineering for Gas Turbines and Power*, **124**:481-488. http://dx.doi.org/10.1115/1.1473153

Chen, H.J., Zhang, B.Z., Su, X.Y., 2003. Low frequency oscillatory flow in a rotating curved pipe. *Journal of Zhejiang University-SCIENCE*, **4**(4):407-414. http://dx.doi.org/10.1631/jzus.2003.0407

Crawford, N., Spence, S., Simpson, A., *et al*., 2009. A numerical investigation of the flow structures and losses for turbulent flow in 90 degrees elbow bends. *Proceedings of the Institution of Mechanical Engineers, Part E: Journal of Process Mechanical Engineering*, **223**(1):27-44. http://dx.doi.org/10.1243/09544089JPME206

Fan, J.R., Yao, J., Cen, K.F., 2002. Antierosion in a 90 degrees bend by particle impaction. *AIChE Journal*, **48**(7):1401-1412. http://dx.doi.org/10.1002/aic.690480705

He, Y.L., Zhao, C.F., Ding, W.J., *et al*., 2007. Two-dimensional numerical simulation and performance analysis of tapered pulse tube refrigerator. *Applied Thermal Engineering*, **27**(11-12):1876-1882. http://dx.doi.org/10.1016/j.applthermaleng.2006.12.022

Holley, B., Faghri, A., 2005. Analysis of pulsating heat pipe with capillary wick and varying channel diameter. *International Journal of Heat and Mass Transfer*, **48**(13):2635-2651. http://dx.doi.org/10.1016/j.ijheatmasstransfer.2005.01.013

Iacovides, H., Launder, B.E., Loizou, P.A., *et al*., 1990. Turbulent boundary-layer development around a square-sectioned U-bend measurements and computation. *Journal of Fluids Engineering*, **112**(4):409-415. http://dx.doi.org/10.1115/1.2909418

Kim, S., Park, J.H., Kojasoy, G., *et al*., 2007. Geometric effects of 90-degree elbow in the development of interfacial structures in horizontal bubbly flow. *Nuclear Engineering and Design*, **237**(20-21):2105-2113. http://dx.doi.org/10.1016/j.nucengdes.2007.02.007

Kim, S., Kojasoy, G., Guo, T.W., 2010. Two-phase minor loss in horizontal bubbly flow with elbows: 45 degrees and 90 degrees elbows. *Nuclear Engineering and Design*, **240**(2):284-289. http://dx.doi.org/10.1016/j.nucengdes.2008.08.019

Kolmogorov, A.N., 1949. On the disintegration of drops in a turbulent flow. *Doklady Akademii Nauk SSSR*, **66**:825.

Kuan, B., Yang, W., Schwarz, M.P., 2007. Dilute gas-solid two-phase flows in a curved 90 degrees duct bend: CFD simulation with experimental validation. *Chemical Engineering Science*, **62**(7):2068-2088. http://dx.doi.org/10.1016/j.ces.2006.12.054

Launder, B.E., Spalding, D.B., 1972. Lectures in Mathematical Models of Turbulence. Academic Press, London, UK.

Li, T.W., Pougatch, K., Salcudean, M., *et al*., 2010. Numerical simulation of an evaporative spray in a gas-solid cross-flow. *International Journal of Chemical Reactor Engineering*, **8**(1):A43. http://dx.doi.org/10.2202/1542-6580.2031

Liu, Y., Miwa, S., Hibiki, T., *et al*., 2012. Experimental study of internal two-phase flow induced fluctuating force on a 90 degrees elbow. *Chemical Engineering Science*, **76**:173-187. http://dx.doi.org/10.1016/j.ces.2012.04.021

Moukalled, F., Darwish, M., 2008. Mixing and evaporation of liquid droplets injected into an air stream flowing at all speeds. *Physics of Fluids*, **20**:040804. http://dx.doi.org/10.1063/1.2912127

Njobuenwu, D.O., Fairweather, M., Yao, J., 2012. Prediction of turbulent gas-solid flow in a duct with a 90 degrees bend using an Eulerian-Lagrangian approach. *AIChE Journal*, **58**(1):14-30. http://dx.doi.org/10.1002/aic.12572

Paliwoda, A., 1992. Generalized method of pressure drop calculation across pipe components containing two-phase flow of refrigerants. *International Journal of Refrigeration*, **15**(2):119-125. http://dx.doi.org/10.1016/0140-7007(92)90036-T

Rutten, F., Meinke, M., Schroder, W., 2001. Large-eddy simulations of 90 degrees pipe bend flows. *Journal of Turbulence*, **2**(3):1-14.

Schiller, L., Naumann, A., 1935. A drag coefficient correlation. *Zeitschrift Des Vereines Deutscher Ingenieure*, **77**:318-320.

Shiraishi, M., Ikeguchi, T., Murakami, M., *et al*., 2002. Visualization of oscillatory flow phenomena in tapered pulse tube refrigerators. *AIP Conference Proceedings*, **613**(1):768-775. http://dx.doi.org/10.1063/1.1472093

Spedding, P.L., Benard, E., 2007. Gas-liquid two phase flow through a vertical 90 degrees elbow bend. *Experimental Thermal and Fluid Science*, **31**(7):761-769. http://dx.doi.org/10.1016/j.expthermflusci.2006.08.003

Spedding, P.L., Benard, E., Donnelly, G.F., 2006. Prediction

of pressure drop in multiphase horizontal pipe flow. *International Communications in Heat and Mass Transfer*, **33**(9):1053-1062. http://dx.doi.org/10.1016/j.icheatmasstransfer.2006.05.004

Sroka, L.M., Forney, L.J., 1989. Fluid mixing in a 90-degrees pipeline elbow. *Industrial & Engineering Chemistry Research*, **28**(6):850-856. http://dx.doi.org/10.1021/ie00090a030

Tunstall, M.J., Harvey, J.K., 1968. On effect of a sharp bend in a fully developed turbulent pipe-flow. *Journal of Fluid Mechanics*, **34**(3):595-608. http://dx.doi.org/10.1017/S0022112068002107

Vashisth, S., Grace, J.R., 2012. Simulation of granular transport of Geldart type-A, -B, and -D particles through a 90 degrees elbow. *Industrial & Engineering Chemistry Research*, **51**(4):2030-2047. http://dx.doi.org/10.1021/ie200647e

Wang, C.C., Chen, I.Y., Yang, Y.W., *et al*., 2003. Two-phase flow pattern in small diameter tubes with the presence of horizontal return bend. *International Journal of Heat and Mass Transfer*, **46**(16):2975-2981. http://dx.doi.org/10.1016/S0017-9310(03)00071-1

Wang, C.C., Chen, I.Y., Yang, Y.W., *et al*., 2004. Influence of horizontal return bend on the two-phase flow pattern in small diameter tubes. *Experimental Thermal and Fluid Science*, **28**(2-3):145-152. http://dx.doi.org/10.1016/S0894-1777(03)00033-5

Weske, J.R., 1948. Experimental investigation of velocity distributions downstream of single dust bends. Technical Report NACA-TN-1471, NASA, Washington DC, USA.

Yang, L.W., 2009. Experimental research of high frequency tapered pulse tube cooler. *Cryogenics*, **49**(12):738-741. http://dx.doi.org/10.1016/j.cryogenics.2009.09.002

Yao, L.S., Berger, S.A., 1975. Entry flow in a curved pipe. *Journal of Fluid Mechanics*, **67**(1):177-196. http://dx.doi.org/10.1017/S0022112075000237

Zhang, H., Tan, Y.Q., Yang, D.M., *et al*., 2012. Numerical investigation of the location of maximum erosive wear damage in elbow: effect of slurry velocity, bend orientation and angle of elbow. *Powder Technology*, **217**: 467-476. http://dx.doi.org/10.1016/j.powtec.2011.11.003

Zhang, P.S., Roberts, R.M., Benard, A., 2013. Numerical simulation of turbulent mist flows with liquid film formation in curved pipes using an Eulerian–Eulerian method. *Journal of Fluids Engineering*, **135**(9):091303. http://dx.doi.org/10.1115/1.4024264

中文概要

题　目：模拟研究气液两相在带缩径管的 90°弯管内的流动

目　的：90°弯管广泛应用于工业中的流体输送，但是流体在经过弯头时会由于离心力的作用而导致弯头下游管道内出现流体分布不均的现象，从而影响后续的生产过程。本文将实验和计算流体力学（CFD）模拟的方法结合研究缩径管对经过弯头后的流体整流作用并分析原因，以期为缩径管在工业中的应用提供一定的参考。

创新点：1. 提出在弯头后的管路中增加缩径管来调整流体的方法；2. 在冷模实验数据验证模拟结果的正确性的基础上，根据 CFD 模拟得到的管道内的压力、流体速度、相分布及湍动能分布详细分析了缩径管能起整流作用的原因。

方　法：1. 通过冷模实验所得的压力数据与模拟值进行对比，证明模拟所采用模型的正确性；2. 通过对不同流体入口条件模拟结果的比较，找到缩径管的作用规律；3. 通过 CFD 模拟得到管道内的压力、流体速度、相分布及湍动能，分析缩径管的整流原理。

结　论：1. 模拟所采用的模型可较好地反映管道内的流体流动情况；2. 缩径管能起到很好的整流效果；3. 缩径管可使流体加速，促进流体的快速混合，因此能够使不稳定的流体快速达到稳定状态。

关键词：90°弯管；缩径管；CFD；均匀分布；流体力学